MDPI

Article

Multirod Pumping Approach with Fresnel Lens and Ce:Nd:YAG Media for Enhancing the Solar Laser Efficiency

Joana Almeida [ID], Hugo Costa [ID], Cláudia R. Vistas [ID], Bruno D. Tibúrcio, Ana Matos and Dawei Liang *[ID]

Centre of Physics and Technological Research (CEFITEC), Departamento de Física, NOVA School of Science and Technology, Campus de Caparica, 2829-516 Caparica, Portugal
* Correspondence: dl@fct.unl.pt

Abstract: A multirod Ce:Nd:YAG solar laser approach, using a Fresnel lens as a primary concentrator, is here proposed with the aim of considerably increasing the efficiency of solar-pumped lasers. Fresnel lenses are cost-effective, rendering solar lasers more economically competitive. In this work, solar-pumped radiation collected and concentrated using the Fresnel lens is received by a secondary three-dimensional compound parabolic concentrator which transmits and funnels the light toward the Ce:Nd:YAG laser rods within a water-cooled tertiary conical concentrator that enables efficient multipass pumping of the rods. To explore the full potential of the proposed approach, the performance of various multirod configurations is numerically evaluated. Through this study, configurations with three and seven Ce:Nd:YAG rods are identified as being the most efficient. A maximum continuous wave total laser power of 122.8 W is reached with the three-rod configuration, marking the highest value from a Ce:Nd:YAG solar laser, leading to solar-to-laser conversion and collection efficiencies of 7.31% and 69.50 W/m², respectively. These results represent enhancements of 1.88 times and 1.79 times, respectively, over the previous experimental records from a Ce:Nd:YAG/YAG single-rod solar laser with a Fresnel lens. Furthermore, the above results are also 1.58 times and 1.68 times, respectively, greater than those associated with the most effective three-rod Ce:Nd:YAG solar laser utilizing a parabolic mirror as the main concentrator. The present study also shows the great usefulness of the simultaneous pumping of multiple laser rods in terms of reducing the thermal stress effects in active media, being the seven-rod configuration the one that offered the best compromise between maximum efficiency and thermal performance. This is crucial for the applicability of this sustainable technology, especially if we wish to scale our system to higher power laser levels.

Keywords: multirod; Ce:Nd:YAG; Fresnel lens; solar laser; solar pumping

1. Introduction

Solar-pumped lasers have the unique capacity to directly use the sunlight to generate laser light, bypassing the requirement for artificial pumping sources and decreasing electrical energy usage. This special kind of laser may afford sustainable energy solutions for several laser-based applications, leading to a substantial decrease in the cost of lasers. Since the Sun is the major energy source available in space, shining uninterruptedly, solar-pumped lasers are potentially well-suited for space-based applications, for example free-space optical communication [1], space-to-space [2] or space-to-Earth [3] wireless power transmission, beam-powered propulsion [4], and deflection of asteroids [5]. They also have a promising role to play in sustainable laser-based material processing [6] and fossil-fuel free energy cycles [7]. Solar-pumped lasers could also be fundamental tools for efficient hydrogen production [8] and wireless power feeding of electric vehicles [9].

This renewable technology has experienced noticeable progress over its 60-year history [10–29]. Still, major breakthroughs have occurred in recent years through the pioneering experiments with neodymium-doped yttrium aluminum garnet (Nd³⁺:YAG) doped

with cerium (Ce^{3+}) ions as an active medium for solar-pumped lasers [24–28], apace with innovative multirod solar pumping schemes [26–29]. Nd^{3+}:YAG has been the most common laser medium employed in solar-pumped lasers since their earliest reports [11–18], owing to the successful combination of the thermal and mechanical attributes of the YAG host material with the spectroscopic characteristics of the Nd^{3+} active ion [30]. However, this dopant has a low spectral correlation with the solar spectrum, restraining the solar-to-laser conversion. Cerium (Ce^{3+}) ions serve as a sensitizer for Nd^{3+} ion emission in the YAG host, possessing two prominent and wide absorption bands in the ultraviolet and visible region that overlap well with the higher intensity region of the solar spectrum. Ce^{3+} also has a broad fluorescence band peaking around 530 nm that spans from 500 nm to more than 600 nm, allowing the intersection with some of the strong absorption lines of the Nd^{3+} ion. When pumping the Ce:Nd:YAG medium with solar radiation, efficient energy transfer can occur from Ce^{3+} to Nd^{3+} ions via both radiative and non-radiative mechanisms, further raising the number of Nd^{3+} ions in the excited state [31–33], and, consequently, the solar laser efficiency [24–28]. Records of solar-to-laser conversion efficiency and collection efficiency (defined as the laser output power per square meter of primary concentrator surface area) stand at 4.64% and 41.3 W/m², respectively, reported by Liang et al. in 2022 following the excitation of three Ce:Nd:YAG laser rods simultaneously, inside a single pump cavity at the NOVA FCT solar furnace [26]. Based on this work, in 2024, Sherniyozov et al. [28] developed a numerical model, calibrated and validated with experimental data [26], to evaluate the efficacy of multirod configurations in relation to Ce:Nd:YAG solar laser performance, identifying patterns with three and seven rods as optimum alternatives to replace the classic single laser rods [28]. The simultaneous pumping of multiple laser rods has emerged as crucial for minimizing thermal load issues commonly associated with solid-state lasers. With this type of optical pumping, each laser rod absorbs only a fraction of the highly focused solar radiation that strikes the pumping cavity, lessening the thermally induced effects and enabling the scalability and stability of the laser power [26–29]. Additionally, these systems have proved their potential for high tracking error compensation, rendering them economically advantageous by eliminating the dependence on expensive high-accuracy solar trackers [27]. Initiatives have also been implemented to miniaturize solar-pumped lasers by considerably reducing the dimensions of the solar concentrators and trackers [19,20] or even by discarding them, employing luminescent solar collectors instead [21,22]. The drawback of these systems is the limited solar laser power (at the milliwatt level) and efficiency due to the limited collection area for sunlight harvesting. That is why primary concentrators with elevated concentration ratios, namely parabolic mirrors and Fresnel lenses, are still required for efficient pumping of bulk solid-state laser media [23–29]. Most solar laser experiments with a multirod configuration and Ce:Nd:YAG as gain media have been carried out using heavy and expensive parabolic mirrors as the primary concentrators [26,27,29], including the most efficient Ce:Nd:YAG solar-pumped laser with a three-rod configuration [26]. Despite the noteworthy advances, this limits the potential of solar lasers to be more economically competitive, promoting the need for cost-effective solar concentrators. Flat Fresnel lenses, despite exhibiting chromatic aberration, are lightweight and adequate for mass production, reducing the complexity and cost of solar-pumped lasers. Moreover, the focus of the Fresnel lenses is situated on their rear side, avoiding shadows associated with the laser head assembly at the focus and enabling easy access during experiments. Numerical research on non-flat Fresnel lenses, such as those with an elliptical or dome shape, has shown that the use of this type of lens could significantly lessen chromatic aberration, consequently enhancing energy concentration [34]. However, as far as we know, the commercially available size for dome-shaped Fresnel lenses is limited. Larger non-flat Fresnel lenses, namely with diameters exceeding 1 m, are typically custom-made due to the complexity of and the costs involved in their manufacture to preserve optical quality. This is why flat Fresnel lenses have been employed as primary concentrators in solar-pumped lasers [15–18,24,25]. The main issue with this kind of system involving Fresnel lenses is their susceptibility to movement caused by

wind pressure, impacting the shape and location of the focal spot, making it challenging to maintain consistent solar laser power during experimental work, especially if large Fresnel lenses are adopted. For these reasons, the diameter of the Fresnel lenses used as primary concentrators in solar laser systems, typically, does not exceed 2 m, and the lens is held by a robust mechanical support [15–18]. Attempts have been made to improve the Ce:Nd:YAG solar laser performance using Fresnel lenses [24,25]. In 2023, Cai et al. reached solar-to-laser conversion and collection efficiencies of 3.88% and 38.8 W/m^2, respectively, by using this type of concentrator to end-side-pump a Ce:Nd:YAG/YAG grooved, bonded crystal rod [24]. In 2024, Liang et al. reported the lowest threshold for solar lasers with the highest solar-to-laser conversion efficiency of 2.06% in a fundamental mode regime by combining a Fresnel lens with a small diameter with a thin Ce:Nd:YAG single rod [25]. However, despite the promising results obtained by using different Fresnel lenses, the potential of these systems remains limited by the pumping of only one single-crystal rod [24,25]. This can preclude solar laser systems from being scaled up to higher powers, especially those with Ce:Nd:YAG as active media whose thermal effects are more pronounced with solar pumping compared to Nd:YAG materials [23].

Due to the aforementioned reasons, the present work aims to exploit the potential of the cost-effective flat Fresnel lens combined with the multirod configuration to advance the Ce:Nd:YAG solar-pumped laser efficiency. The system design consists of a standard Fresnel lens, with a 1.5 m diameter and a 2 m focal length, as the primary concentrator and a single laser head composed of a secondary three-dimensional (3D) compound parabolic concentrator (CPC) and a tertiary conical concentrator, within which the Ce:Nd:YAG laser rods are end-side-pumped. With this technique of optical pumping, the majority of the concentrated solar radiation is collected by the end face of the laser rods, i.e., parallel to the laser beam, enabling a higher pumping efficiency compared to the side-pumping scheme [15–19,24–26]. To explore the potential of the proposed laser system for maximum solar-to-laser conversion, various multirod arrangements with different number of laser rods are numerically analyzed. Configurations with three Ce:Nd:YAG rods lead to the highest laser power extraction in continuous wave (cw) and, consequently, to the highest solar-to-laser conversion and collection efficiencies of 7.31% and 69.50 W/m^2, respectively. Nonetheless, by adopting a seven-rod configuration, with smaller-diameter laser rods, the laser system efficiency is also high, reaching 7.28% and 69.16 W/m^2 solar-to-laser conversion and collection efficiencies, respectively, with the benefit of reducing considerably the thermal stress effects in the active media.

2. Multirod Ce:Nd:YAG Solar Laser System with a Fresnel Lens

As shown in Figure 1, the Fresnel lens with a 1.5 m diameter (1.767 m^2 collection area) and a 2.0 m focal length was used to collect and focus the incoming solar rays toward the laser head.

The specifications of the present Fresnel lens are indicated in Table 1. The Fresnel lens was made of polymethyl methacrylate (PMMA), which has a density of approximately 1.18 g/cm^3. It is a lightweight and resilient polymer that offers high transmission in the solar wavelength range, making these lenses more resistant to solar exposure and stable at temperatures up to 80 °C [35]. By considering the full solar spectrum, a transmission efficiency of 78% was numerically determined.
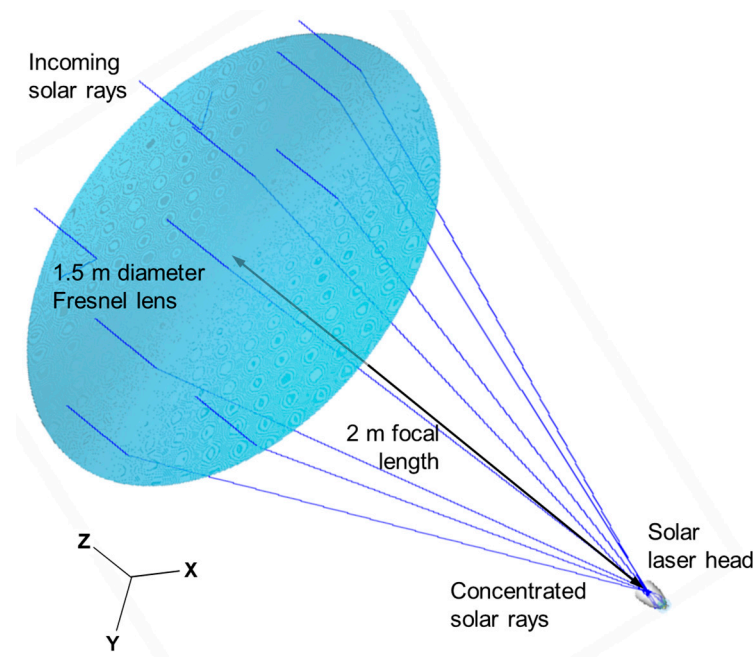
Figure 1. Schematic design of the multirod solar laser system with the 1.5 m diameter Fresnel lens as the primary concentrator.

Table 1. Specifications of the Fresnel lens primary concentrator.

Material	PMMA
Radius, r_{FL}	0.75 m
Focal length, f_{FL}	2.0 m
f-number	1.33
Thickness	5 mm
Pitch, Δr	850 μm
Transmission efficiency	78%
Weight	102.2 N

Fresnel lenses are typically flat, featuring one smooth surface and one grooved surface. The grooved side consists of multiple concentric prisms that function as a lens, focusing sunlight. The segmentation of the Fresnel lens into several small prisms saves more optical material, lowering system costs compared to conventional lenses. However, this segmentation introduces diffraction through the edges of these prisms, causing some light to spill outside the target area, resulting in energy losses of the system [36,37].

The relative amount of incoming solar power that misses the solar laser head due to diffraction ($P_{\text{loss}}/P_{\text{inc}}$) by the prism facets of the Fresnel lens can be approximately estimated through Equation (1) [36]:

$$\frac{P_{\text{loss}}}{P_{\text{inc}}} \approx \frac{4\sqrt{C_{\text{geo}}}}{5\pi k \Delta r} \frac{\left(1 + \tan^2\phi\right)^{5/2} - 1}{\tan^3\phi} \tag{1}$$

Here:

- C_{geo} denotes the geometrical concentration, defined as the ratio of the Fresnel lens area to the target area. In the present case, the target is the 3D-CPC input aperture with radius $r_{\text{target}} = 32$ mm. As both areas are circular, $\sqrt{C_{\text{geo}}}$ equals the ratio of the radii of these areas (r_{FL} and r_{target}).
- $k = 2\pi/\lambda$ is the wavelength number of the incoming solar light.
- Δr is the pitch.

- $\tan\phi = r_{FL}/f_{FL}$.

Based on this analytical approximation [36], the optical losses caused by the diffraction generated by the present Fresnel lens were calculated. As shown in Figure 2, the diffraction losses were well below 1% within the whole spectral range relevant to the pumping of the Ce:Nd:YAG media.
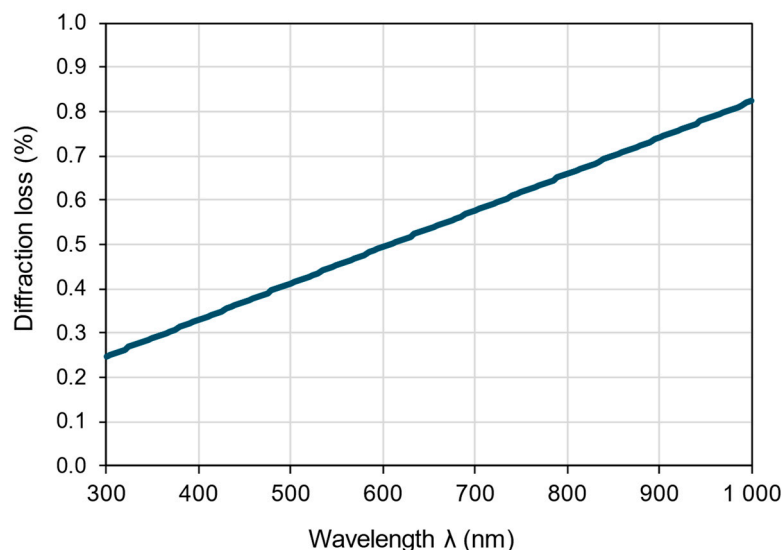

Figure 2. Diffraction losses of the Fresnel lens primary concentrator with a 0.75 m radius, a 2.0 m focal length, and an 850 µm pitch, concentrating the light on the 3D-CPC entrance with a 32 mm radius. The analytical calculation was based on Equation (1), adapted from [36].

The solar laser head consisted of the secondary 3D-CPC and the tertiary conical concentrator, within which the Ce:Nd:YAG laser rods were fixed and cooled by water. As illustrated in Figure 3a, the solar radiation concentrated at the focus of the 1.5 m Fresnel lens was collected and funneled by the dry 3D-CPC, which has an acceptance angle of 28°, input/output diameters of 64 mm/30 mm, and a height of 88 mm. The 3D-CPC is founded on the CPC design concept for flat receivers, utilized to transform rays from a large input aperture, receiving a smaller angle, into a narrower output aperture, emitting at a wider angle. This means that the irradiance is higher at the concentrator output aperture [38], enabling efficient focusing of the pump radiation toward the laser media. An aspheric fused silica lens with a 30 mm output diameter, a 35 mm radius of curvature, a 1.0 conic constant, and a 10 mm thickness was implemented at the output aperture of the 3D-CPC to effectively concentrate the solar radiation into the laser rods, as depicted in Figure 3b. The 3D-CPC, paired with the aspheric fused silica lens at its output end, enabled the transfer of 92% of the concentrated solar power at its input to the entrance aperture of the conical cavity.

Fused silica material is well-suited for solar-pumped lasers owing to its broad transparency range across the laser gain media absorption spectrum. It also has a strong resistance to high temperatures and thermal shock [39]. The aspheric lens also acted as a cap, preventing water from entering the 3D-CPC.

The conical concentrator filled with water, illustrated in more detail in Figure 3c, was then used to confine the light through several reflections, enabling the multipass pumping of the laser rods. The laser rods were positioned approximately 4 mm away from the 3D-CPC output aperture to ensure the effective cooling of the end-side-pumped active media, especially along their top region where most of the concentrated solar rays were received.
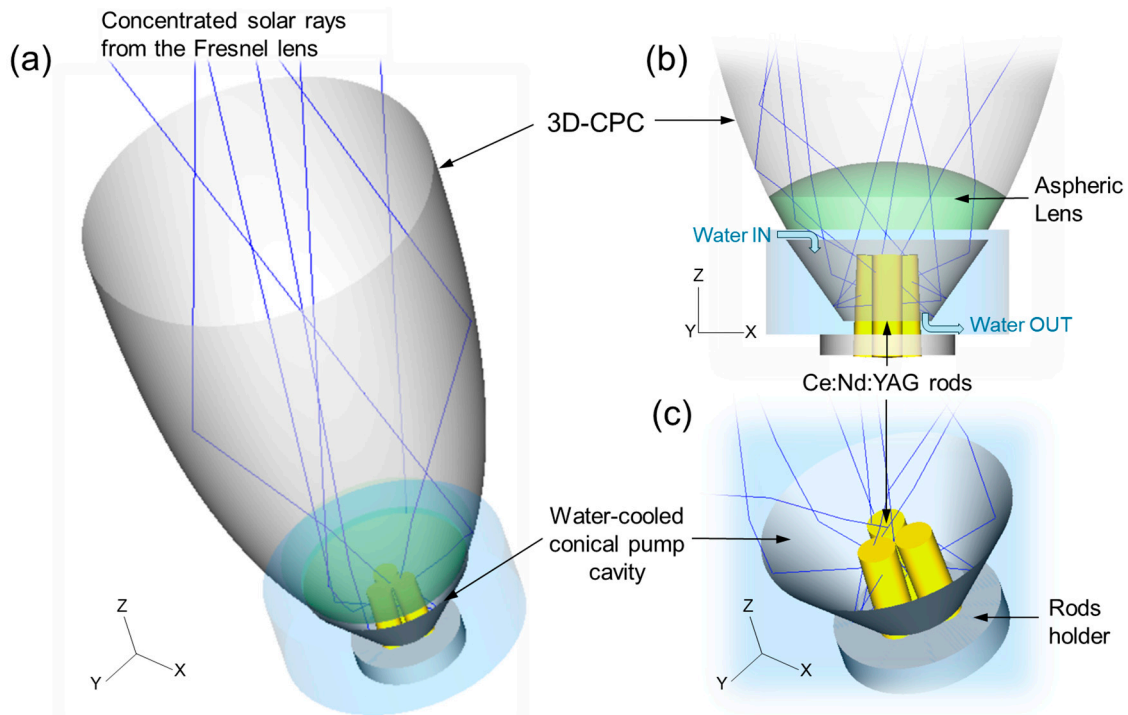
Figure 3. (**a**) Schematic layout of the solar laser head composed of the dry 3D-CPC, the aspheric lens, the water-cooled conical cavity, and the three Ce:Nd:YAG rods. (**b**) Two-dimensional view of the 3D-CPC output section, with the aspheric lens incorporated and the conical concentrator with the three rods inside it. (**c**) Detailed 3D view of the optical pumping of the laser rods by the conical cavity. The 3D-CPC and aspheric lens were not drawn for better visualization.

The conical cavity in Figure 3 had a 30 mm input diameter and a 13 mm output diameter and a 12 mm height, having been optimized for a three-rod configuration in which each Ce:Nd:YAG rod had a 4.5 mm diameter and a 15 mm length. The laser rods were inclined in a rotationally symmetric manner with respect to the *z*-axis, allowing, on the one hand, their upper sections to be as close as possible for maximum collection of the solar rays from the 3D-CPC output aperture and, on the other hand, their end sections to be far enough apart for mechanical fixation in the common holder with a 3 mm thickness.

The proposed solar laser system could be incorporated into a two-axis solar tracker structure, thus operating in direct tracking mode [16].

3. Numerical Modeling of Several Multirod Configurations

The design specifications of the present solar laser approach were initially optimized using the Zemax® 13 ray-tracing software in the non-sequential mode to maximize the pump power absorbed by each laser rod. The LASer Cavity Analysis and Design (LASCAD^TM) software (version 3.3.5) was subsequently used to determine the optimal laser resonator parameters for maximum solar laser extraction.

To design the solar laser scheme, the elements were specified using the non-sequential objects of Zemax® 13 within the Component Editor window [40]. The 1.5 m diameter Fresnel lens captured and focused the solar rays coming from two circular solar sources that had the same area (*A*) of 1.767 m^2, equivalent to the collection area of the Fresnel lens. One of the light sources (source 1) characterized the most significant wavelengths from the Sun that coincide with the absorption spectrum of Nd^{3+} ions and those associated with the non-radiative transition from Ce^{3+} to Nd^{3+} via quantum cutting [32], while the other source (source 2) represented the solar emission wavelengths concerning the radiative transfer from Ce^{3+} to Nd^{3+}. To accomplish this, the wavelength information was divided into two spectrum datasets, corresponding to each source [40]. The spectrum dataset for source 1 resembled the wavelength data from previous Nd:YAG solar laser studies [40], i.e.,

with a total of 22 dominant absorption wavelengths defined for Nd^{3+}, whose contribution is evaluated according to its spectral irradiance level within the reference one-and-a-half air mass (AM1.5 D) direct solar spectrum [41]. In the spectrum file of source 2, six wavelengths were specified, corresponding to the key Nd^{3+} peak absorption wavelengths matching the Ce^{3+} fluorescence spectrum: 527 nm, 531 nm, 569 nm, 579 nm, 586 nm, and 592 nm [26]. In this instance, the weight of each wavelength was based on its spectral intensity in the Ce^{3+} fluorescence spectrum [40]. The power of source 1 ($P_{source1}$) and source 2 ($P_{source2}$) was calculated by using Equations (2) and (3), respectively [40]:

$$P_{source1} = A \times I_S \times \left(\eta_{overlap,Nd^{3+}} + \eta_{overlap,Ce^{3+}} \times \eta_{NR:Ce^{3+} \rightarrow Nd^{3+}} \right) \tag{2}$$

$$P_{source2} = A \times I_S \times \eta_{overlap,Ce^{3+}} \times \eta_{R:Ce^{3+} \rightarrow Nd^{3+}} \tag{3}$$

Here:

- A denotes the collection area of the primary concentrator, i.e., 1.767 m^2.
- I_s is the terrestrial solar irradiance.
- $\eta_{overlap,Nd^{3+}}$ is the spectral overlap between the Nd^{3+} absorption spectrum and the solar emission spectrum, i.e., 16% [40].
- $\eta_{overlap,Ce^{3+}}$ is the spectral overlap between the Ce^{3+} absorption spectrum and the solar emission spectrum, i.e., 15.3% [40].
- $\eta_{NR:Ce^{3+} \rightarrow Nd^{3+}}$ is representative of the proportion of energy absorbed by Ce^{3+} ions that could be transferred non-radiatively to Nd^{3+}, i.e., 70% [31].
- $\eta_{R:Ce^{3+} \rightarrow Nd^{3+}}$ is the fraction of energy absorbed by Ce^{3+} ions that could be transferred radiatively to Nd^{3+}, i.e., 30% [31].

Considering a peak solar irradiance of 950 W/m^2 in the Lisbon area, on clear sunny days [40], $P_{source1}$ = 448.4 W and $P_{source2}$ = 77 W were calculated.

To define the Ce(0.1 at.%):Nd(1.1 at.%):YAG material, the abovementioned 22 peak absorption wavelengths of Nd^{3+} and the corresponding absorption coefficients were incorporated into the glass catalog in Zemax® 13. To account for absorption losses in the active media, the wavelength-dependent refractive indices and absorption spectra of PMMA, fused silica, and water materials were also added to the glass catalog data. For the 3D-CPC and conical cavity inner walls, a 95% reflectivity was assumed.

To ascertain the potential of the proposed laser system for maximum solar-to-laser energy conversion, its performance was evaluated for different multirod configurations, with different numbers of rods, ranging from three to seven rods, as it can be seen in Figure 4. For the configurations with three, four, and five rods, as well as for one of the configurations with six rods, all the laser rods were evenly arranged in rotational symmetry around a common central axis to guarantee an even distribution of the pump light, as illustrated in Figure 4b. This arrangement also allowed for the compactness of the laser rods, namely for the three-, four-, and five-rod configurations. Nonetheless, as the number of rods increased, the central dead space became larger, a phenomenon which was especially evident in the six-rod configuration, hampering pump efficiency [28]. Therefore, we also decided to evaluate the performance of a six-rod configuration with a different arrangement of the laser rods for comparison, with one central rod and five external rods of the same dimension rotated symmetrically around it. Still, this configuration led to more dead spaces between the external rods, as shown in Figure 4b. By increasing the number of external rods to six, a more compact packing of the laser rods, and, consequently, an effective collection of the concentrated solar energy at the entrance of the pumping cavity was ensured [28]. For this reason, the performance of the present solar laser system was also analyzed by using a seven-rod configuration, with one central rod and six external rods. For each multirod configuration, the Ce:Nd.YAG laser rod dimensions, as well as the angle of inclination (α) of the laser rods in relation to the z-axis, were optimized to find out the maximum absorbed pump power for each one. Thus, the upgrade of each configuration implied redesigning the conical concentrator.
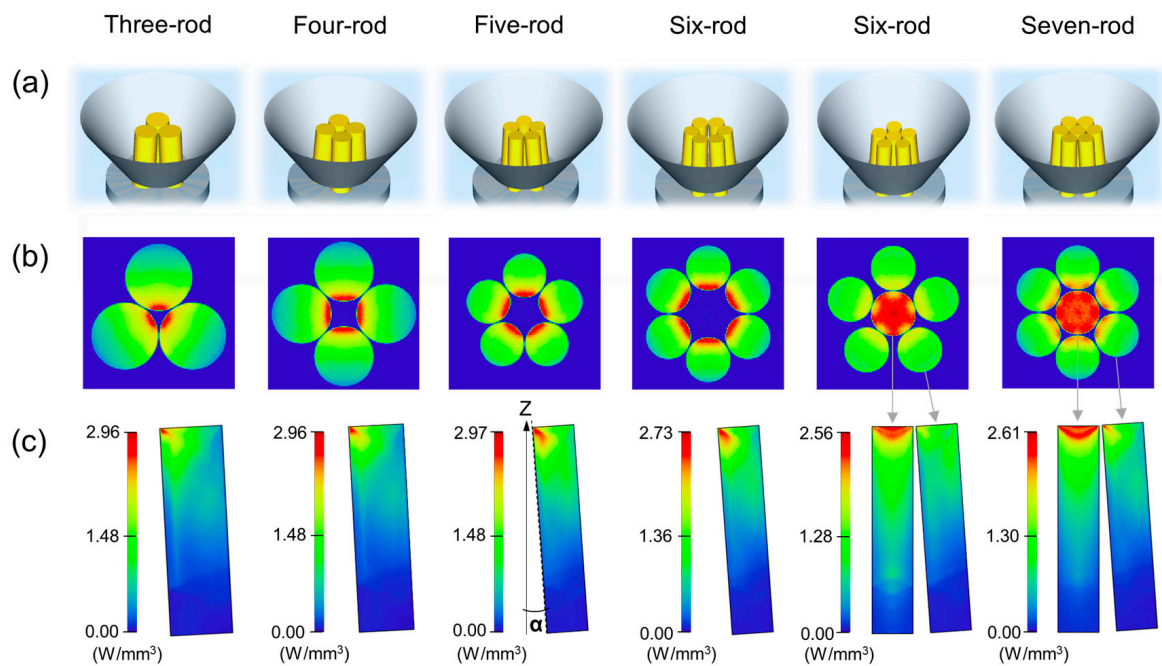
Figure 4. (**a**) Multirod pumping configurations with a different number of Ce:Nd:YAG laser rods. (**b**) Absorbed pump flux distributions in the upper transversal cross-sections of the laser media and (**c**) the central longitudinal cross-sections of one of the laser rods with rotational symmetry. For the seven-rod and one of the six-rod configurations, the absorbed pump flux distribution in the central rod is also given. The term α represents the angle of inclination of the Ce:Nd:YAG laser rods in relation to the *z*-axis.

To analyze the absorbed pump power and pump distribution in the Ce:Nd:YAG laser media, a detector volume consisting of thousands of voxels was utilized for each rod. During the ray-tracing process, the optical path taken by the rays in each voxel was determined. The absorbed pump flux in each voxel was calculated based on this information, along with the effective absorption coefficient of the 1.0 at.% Nd^{3+}:YAG material. The overall absorbed pump power was then found by summing up the absorbed pump flux across all voxels. The accuracy of the numerical results and image resolution of the detector can be upgraded by increasing the number of voxels together with the number of analysis rays. Nevertheless, when changing these parameters, it is important to consider their impact on the total time needed for each simulation.

Examples of the acquired absorbed pump flux distributions by the Ce(0.1 at.%):Nd(1.1 at.%):YAG rods with a 15 mm length at different configurations are shown in Figure 4. The red and blue colors identify the regions of the rods where there is maximum and minimum pump absorption, respectively. The absorbed pump flux distributions in the upper transversal cross-sections of the laser media are presented in Figure 4b, whereas Figure 4c shows the absorbed pump flux distributions in the central longitudinal cross-sections of one the laser rods rotated symmetrically. The longitudinal absorbed pump flux distributions of the central rods of the six-rod and seven-rod configurations are also given. As expected, the laser media had rotational symmetric absorbed pump flux profiles, with a higher intensity in the upper section and in proximity of the *z*-axis. A more intense absorbed pumping distribution was also obtained for the central Ce:Nd:YAG rods from both the six-rod and the seven-rod configurations.

The absorbed power distribution data from each laser rod was subsequently imported into the LASCAD^{TM} 3.3.5 software to evaluate the thermal effects in the gain medium and the laser output power. An optical resonator was hence formed for each Ce:Nd:YAG rod, consisting of two parallel mirrors facing each other at right angles to the laser rod's axis, as illustrated in Figure 5. The leftmost mirror is representative of the high reflection (HR)

coatings at the laser emission wavelength (1064 nm, 99.9%) on the upper face of the laser rod, while the rightmost mirror is representative of the partial reflection (PR, 1064 nm) output coupler. The amount of feedback is governed by the reflectivity of the PR mirror, which varied between 90% and 99% in the present scheme. The end faces of the laser rods closer to the PR mirrors had an antireflective (AR) coating at 1064 nm, also illustrated in Figure 5.
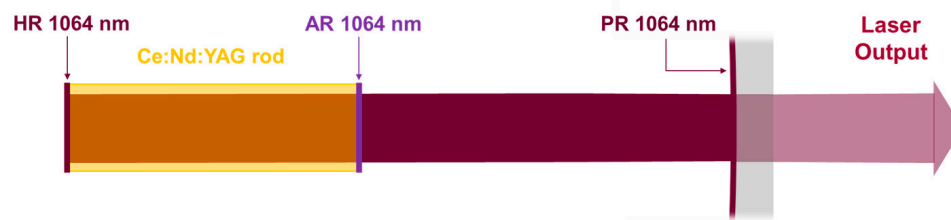
Figure 5. Schematic design of one of the solar laser resonators from the multirod configurations, consisting of the high reflection (HR) mirror, the Ce:Nd:YAG active medium, and the partial reflection (PR) mirror, operating under the multimode regime. The image is not at scale.

To assess the maximum laser power that might be extracted by each laser rod, plane-concave short laser resonators were chosen [16,26], where the distance from the PR mirror to the laser rod did not exceed 100 mm, ensuring that the energy of higher-order modes was not significantly affected by diffraction losses.

In the LASCAD™ 3.3.5 numerical analysis, a fluorescence lifetime of 230 µs, a stimulated emission cross-section of 2.8×10^{-19} cm^2, and a typical absorption and scattering loss of 0.002 cm^{-1} [26] were considered. The mean absorbed and intensity-weighted solar radiation wavelength of 660 nm [13] was also adopted.

The specifications of the Ce:Nd:YAG crystal rods are summarized in Table 2.

Table 2. Specifications of the Ce:Nd:YAG crystal rods.

| **Doping Concentration**	**Ce:0.1 at%, Nd:1.1 at%**
Orientation	<111>
Parallelism	$\leq 10''$
Perpendicularity	$\leq 5'$
Flatness	$\lambda/10$ @632.8 nm
Laser wavelength	1064 nm
Coatings	HR (R $\geq$ 99.9% @1064 nm) AR (R < 0.2% @1064 nm)
Refractive index	1.8197 @1064 nm
Stimulated emission cross-section	2.8×10^{-19} cm^2
Fluorescence lifetime	230 µs
Absorption and scattering loss	0.002 cm^{-1}

4. Numerical Results of the Multirod Ce:Nd:YAG Solar Laser Performance

The influence of the laser rod diameter (D) and length (L) on the laser output power from the Ce:Nd:YAG solar laser approach was first evaluated for the three-rod configuration, as shown in Figure 6. The highest total cw laser power of 122.8 W was numerically found for the set of three rods with D = 4.5 mm and L = 15 mm, meaning that each rod emitted simultaneously 40.93 W cw laser power. With the elongation of the rods, the laser power decreased, and its maximum value tended to shift toward smaller diameter rods. For example, for L = 25 mm, the maximum total cw laser power of 117.7 W was numerically obtained from the laser rods with D = 3.5 mm. For shorter L = 12.5 mm rods, the laser power dropped more abruptly, especially for smaller-diameter rods. The maximum total cw laser power of 118.3 W was achieved, in this case, from the rods with D = 4.5 mm.
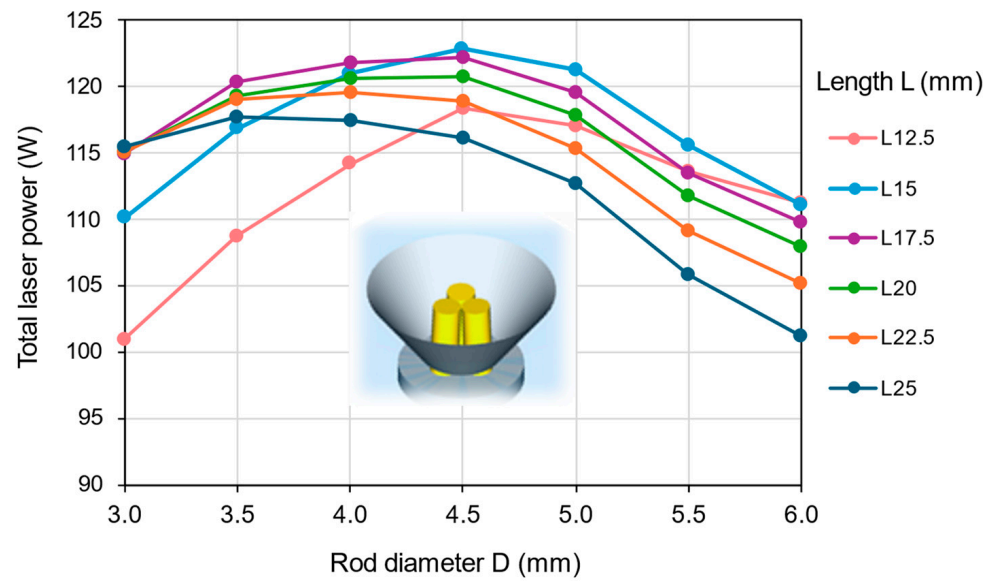
Figure 6. Total cw laser output power as a function of the laser rod diameter (D) and length (L) for the Ce:Nd:YAG solar laser scheme with a three-rod configuration.

To exploit the full potential of the proposed scheme, the maximum laser power that could be extracted from the six different multirod configurations, presented in Section 3, was numerically analyzed, as shown in Figure 7. The laser rod diameter (D) was optimized for each one, while the laser rod length was fixed at 15 mm.
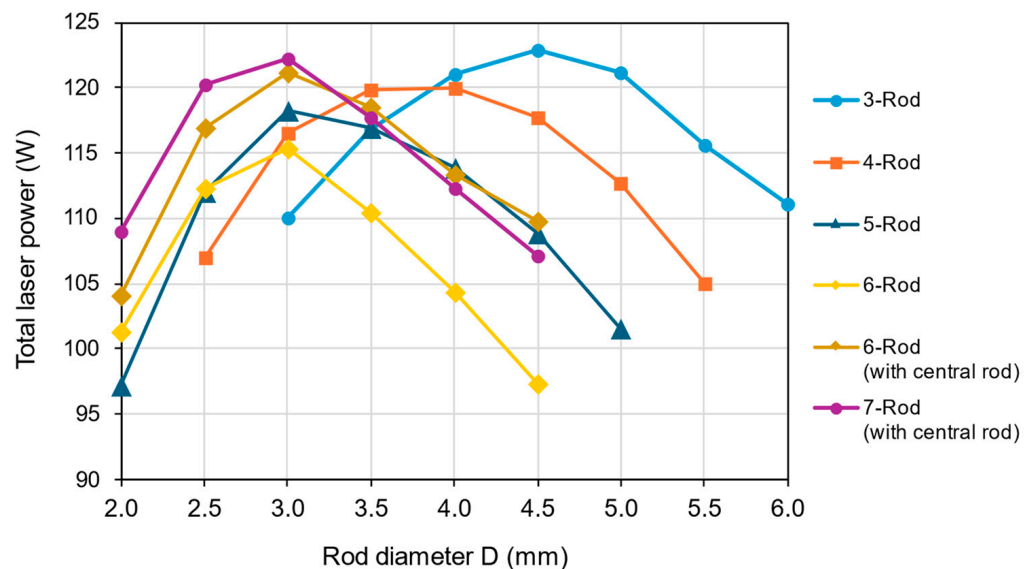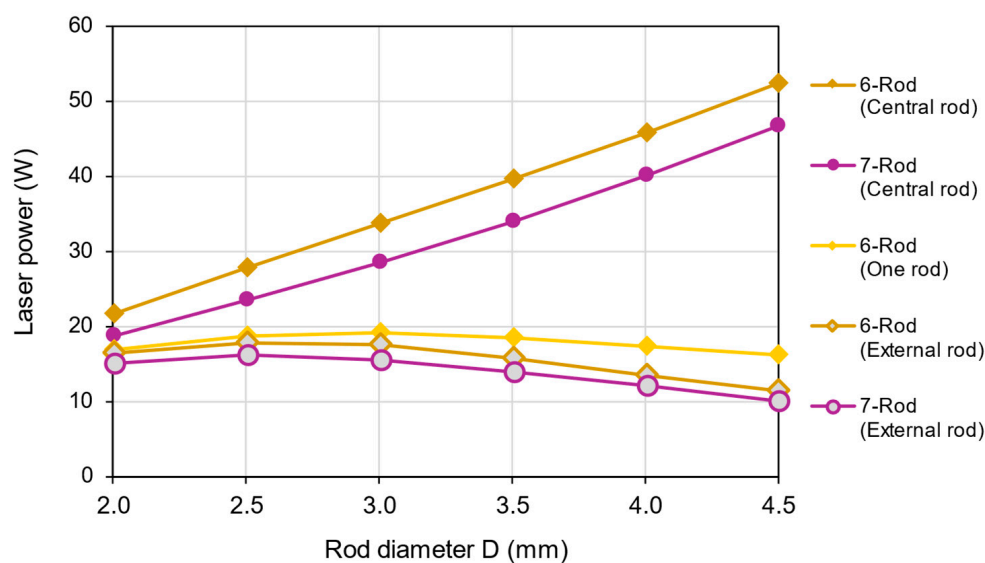

Figure 7. Total cw solar laser power as a function of the rod diameter (D) for six different multirod configurations, with the number of rods ranging from three to seven. The laser rods length was fixed at 15 mm.

Among the configurations without a central rod, the three-rod configuration is the one that offered the maximum total cw solar laser power of 122.8 W, with D = 4.5 mm. As the number of Ce:Nd:YAG rods increased, an overall decrease in laser power was observed, which can be attributed to the enlargement of the central gap among the laser rods, demonstrated in Figure 4b, which limits the pump energy to effectively reach each laser rod. Even so, the solar laser extraction from thinner laser rods tended to increase with the addition of more laser rods, as indicated in Figure 7. For example, for the five-rod configuration, the maximum total cw laser power of 118.2 W was numerically produced

from rods with D = 3.0 mm, while, for the four-rod and three-rod configurations presenting rods with the same diameter, the total cw laser power dropped to 116.6 W and 110.1 W, respectively. As for the six-rod configuration without a central rod, the highest total cw laser power obtained was 115.4 W, again by using rods with D = 3.0 mm. Although it was lower than that obtained from the four- and five-rod configurations, it had an additional total power of 5.3 W in relation to that from the three-rod configuration with rods of the same diameter. In addition, when the six rods were rearranged, evenly placing five rods around a central rod, the total cw laser power increased substantially to 121.2 W, surpassing the maximum values from the five-rod and four-rod configurations. By increasing the number of external rods to six, the gaps between the laser rods were reduced, leading to an improvement in the total cw laser power to 122.2 W. This value is very close to the highest total laser power reached by the solar laser system with three Ce:Nd:YAG rods of larger diameter, proving that the seven-rod configuration can be as efficient as the three-rod configuration, with the additional advantage of being more effective in reducing the thermal effects in the active media.

The main issue encountered when using the seven-rod configuration, as well as when using the six-rod configuration with a central rod, was the uneven sharing of the concentrated sunlight between the central rod and the external rods, as already shown in Figure 4b,c. In both configurations, the central rod presented a more intense absorption profile compared to the external ones, causing them to make a greater contribution to laser extraction. Figure 8 shows the cw solar laser powers from the central rod and from one of the external rods of the six-rod and seven-rod configurations as a function of rod diameter (D). The cw solar laser power produced by one of the six laser rods of the configuration without a central rod is also given for comparison.

Figure 8. Solar laser power produced by the central rod and by one of the external rods of the six- and seven-rod configurations as a function of rod diameter (D). The cw solar laser power produced by one of the six rods of the configuration without a central rod is also given for comparison.

As it can been seen in Figure 8, the contribution of the central rods to laser power production grew with increasing rod diameter, and the discrepancy between the laser powers from the central and external rods was most notable in the six-rod configuration. The inclusion of the central rod also impaired the absorption of the solar rays by the rods with rotational symmetry, leading to a reduction in the laser power emitted by each external rod of the six- and seven-rod configurations compared to that of the six-rod configuration without a central rod. This reduction was also more pronounced with increasing rod diameters.

Due to the greater contribution of the central laser rods to the absorption of pumping radiation compared to the external rods, the thermal stress effects were also more pronounced in the central rods, becoming stronger with increasing rod diameters, as observed in Figure 9. The thermal stress effects were also more noticeable in the six-rod than in the seven-rod configuration.
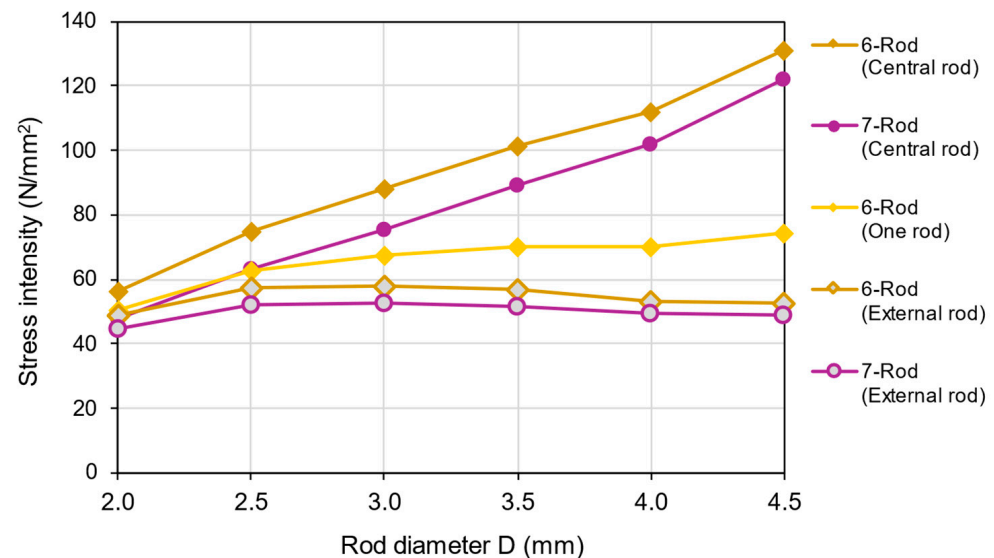
Figure 9. Maximum stress intensity in the central rod and in one of the external rods of the six- and seven-rod configurations as a function of the rod diameter (D). The maximum stress intensity obtained by one of the six rods of the configuration without a central rod is also given for comparison.

To overcome this drawback, it is, therefore, very important to adopt multirod configurations with thin laser rods. As a matter of fact, it was already proven in Figure 7 that the performance of the present solar laser system with five, six, and seven laser rods was at its maximum when the laser rods had a diameter which did not exceed 3.0 mm.

The angle of inclination (α) of the Ce:NdYAG laser rods in relation to the *z*-axis was also an important parameter in relation to the optimization of the solar laser system for maximum laser extraction. As it can been seen in Figure 10, for each set of laser rods there was also an optimal α, which tended to increase as the number of rods grew. For the three-rod configuration, the highest total laser power of 122.8 W was produced with the rods inclined 2.5° in rotational symmetry with respect to the *z*-axis, while, for the four-rod configuration, $\alpha = 3.0°$ offered the maximum laser power of 120 W. For the five-rod and seven-rod configurations, the optimal angle of inclination shifted to $\alpha = 4.0°$, resulting in the total laser powers of 118.2 W and 122.2 W, respectively. The same optimal angle was also found for the six-rod configuration with no central laser rod, leading to a 115.4 W total power. However, for the six-rod configuration with a central rod, the variation of the external rod's inclination had only a tenuous effect on the maximum laser power of 121.2 W, namely when α varied between 1.0° and 5.0°. We believe that this was due to the dead spaces between the five external rods, illustrated in Figure 4b, as such a configuration permits less variation in the repositioning of the rods with the variation of α, and, consequently, less variation in the absorbed pump power, compared to the other configurations whose rods were more compacted. The minor influence of the external rods on the laser power production compared to that of the central rod, as shown in Figure 8, may have also contributed to the weaker effect of α on the total laser power in the six-rod configuration.
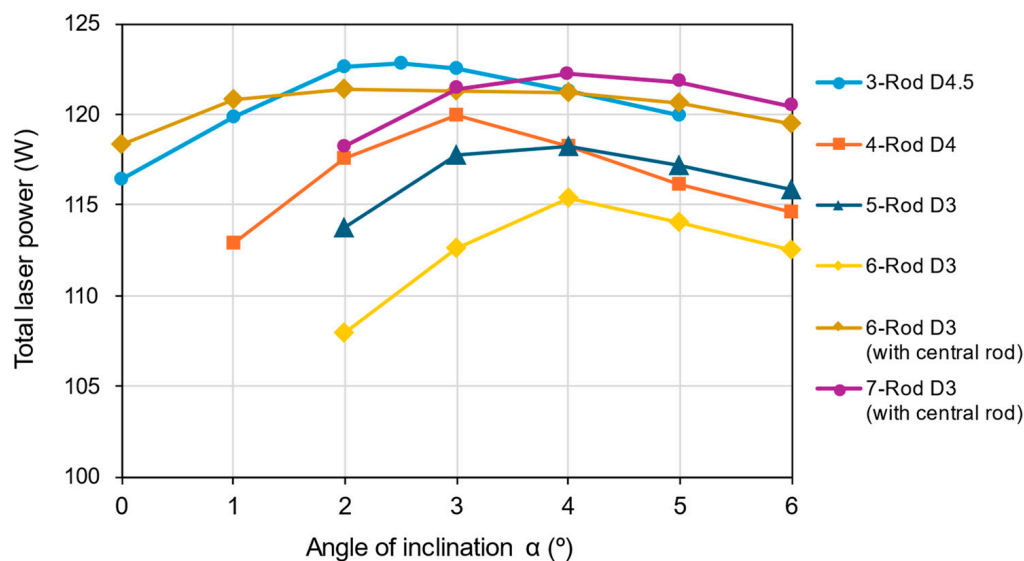
Figure 10. Total cw solar laser power as a function of the angle of inclination of the rods (α) for each configuration with optimal rod diameter (D).
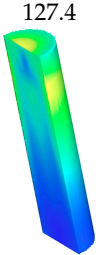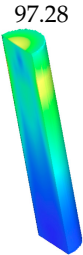
5. Discussion

Table 3 outlines the optimal results in terms of laser power, efficiency, and thermal performance that were numerically obtained from the proposed scheme for each multirod configuration. The maximum total cw laser power of 122.8 W was attained from the three-rod configuration, re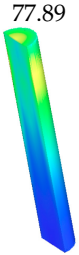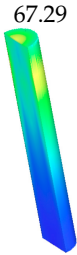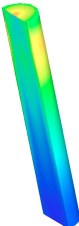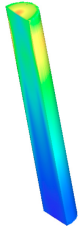sulting in the highest solar-to-laser conversion and collection efficiencies of 7.31% and 69.50 W/m^2, respectively. The present solar laser system also performed quite well using a seven-rod configuration, producing a maximum total laser power of 122.2 W, which was less than 1% lower than the highest value. Therefore, high collection and solar-to-laser conversion efficiencies of 69.16 W/m^2 and 7.28% were also reached with the seven-rod configuration. Based on these outcomes, we can conclude that the configurations with three and seven rods were the ones that performed best, such results being in agreement with the previous study by Sherniyozov et al. [28] using a parabolic mirror as the primary concentrator. However, in terms of thermal performance, the three-rod configuration was the most affected, attaining the highest maximum stress intensity of 127.4 N/mm^2 for each one of the laser rods. The seven-rod configuration, with maximum stress intensities of 75.61 N/mm^2 and 52.56 N/mm^2 for the central rod and each one of the six external rods, respectively, was the one that performed best in relation to all configurations, except for the six-rod configuration without a central rod. In this configuration, a maximum stress intensity of 67.29 N/mm^2 was numerically obtained for each one of the six rods, such a value being the lowest value compared to those from the configurations without a central rod. It was also lower than that of the central rods of the six- and seven-rod configurations.

In end-side-pumping schemes, the inhomogeneous pump distribution over the active medium may potentially cause excessive heat buildup in the laser rod, a phenomenon which is particularly concerning for solar laser systems that rely on just one large crystal for pumping. The high thermal load in the laser rod can induce not only common thermal effects, such as thermal lensing, stress, and birefringence, but also thermal population of lower laser levels, a phenomenon often disregarded in solar-pumped lasers, but which could exert a significant influence on their performance [42]. The adoption of multirod pumping configurations, especially with small-diameter laser rods, may provide an optimal solution to overcome the thermal challenges in solar-pumped lasers [42,43]. Configurations with a higher number of rods pose more practical challenges, but the amount of concentrated sunlight that is received by each rod can be significantly reduced and used more efficiently by thinner rods, possibly leading to the substantial reduction of the thermal

stress effects in the active media, as confirmed by Table 3. Future upgrades in relation to the thermal performance and efficiency of solar lasers might also be possible through the incorporation of composite laser rods, such as YAG/Ce:Nd:YAG/YAG, in multirod systems [43].

Table 3. Overview of the Ce:Nd:YAG solar laser performance with different multirod configurations.

Design configuration						
Number of rods	3	4	5	6	6	7
Rods diameter (mm)	4.5	4.0	3.0	3.0	3.0	3.0
Maximum total laser power (W)	**122.8** (3 × 40.93)	120.0 (4 × 29.99)	118.2 (5 × 23.65)	115.4 (6 × 19.23)	121.2 (5 × 17.49 + 33.73)	**122.2** (6 × 15.60 + 28.57)
Solar-to-laser conversion efficiency (%)	**7.31**	7.15	7.04	6.87	7.22	**7.28**
Collection efficiency (W/m^2)	**69.50**	67.91	66.89	65.31	68.59	**69.16**
Maximum stress intensity (N/mm^2)	127.4	97.28	77.89	67.29	Central rod: 88.06 External rod: 58.09	Central rod: 75.61 External rod: 52.56

Following the initial report on simultaneous emissions from three Nd:YAG rods [29], our research team has conducted extensive numerical studies on multirod pumping schemes, some of them including the use of flat Fresnel lenses as primary concentrators [44–47], as summarized in Table 4.

The main goal of the studies by Liang et al. [44] and Costa et al. [47] was to maximize the solar laser efficiency in fundamental mode (TEM$_{00}$ mode). In both cases, Fresnel lenses featuring a large effective total collection area were used to pump seven rods within a single pumping cavity. However, in the first study, a single large Fresnel lens was used to end-side pump the seven rods, with Nd:YAG as the laser material [44], while, in the second study, twelve sets of folding mirrors and Fresnel lenses were employed to collect and concentrate the solar radiation to side pump the seven Ce:Nd:YAG rods [47]. In relation to the other two studies [45,46], the solar laser was optimized to operate in multimode conditions, as in the present case. Nonetheless, these studies were mainly focused on achieving steady and

uniform solar laser emission under the influence of solar tracking error via two different pumping arrangements, end-side pumping [45] and side pumping [46], with different numbers of Nd:YAG laser rods. The present study is the first to explore the potential of an end-side-pumped multirod configuration with Ce:Nd:YAG active media paired with a simple Fresnel lens primary concentrator to boost solar laser efficiency by using a more economically viable system for solar collection and concentration compared to earlier works [44,46,47]. With that goal in mind, an innovative double-stage concentrator, combining a 3D-CPC and a conical cavity, was also proposed to enhance the capture of the concentrated sunlight and its effective delivery to the laser rods. Furthermore, this is the first numerical work that thoroughly analyzes the influence of the number of rods and their arrangement on the performance of the solar laser with a Fresnel lens.

Table 4. Overview of the current multirod Ce:Nd:YAG solar laser performance and its comparison with previous numerical works incorporating Fresnel lenses and multirod configurations [44–47].

Parameters	Numerical Work				
	Liang et al., 2021 [44]	Vistas et al., 2023 [45]	Tibúrcio et al., 2023 [46]	Costa et al., 2024 [47]	Present Work
Number of Fresnel lenses	1	1	2	12	1
Effective collection area	4.0 m^2	1.767 m^2	3.53 m^2	6.0 m^2	1.767 m^2
Rod material	Nd:YAG	Nd:YAG	Nd:YAG	Ce:Nd:YAG	Ce:Nd:YAG
Number of rods	7	6	4	7	From 3 to 7
Pumping configuration	End-side pumping	End-side pumping	Side pumping	Side pumping	End-side pumping
Regime	TEM_{00} mode	Multimode	Multimode	TEM_{00} mode	Multimode
Maximum total solar laser power	54.65 W	34 W	104.4 W	212.39 W	122.8 W
Maximum solar-to-laser conversion efficiency	1.44%	2.0%	2.96%	3.73%	7.31%
Maximum collection efficiency	13.66 W/m^2	19.24 W/m^2	29.7 W/m^2	35.40 W/m^2	69.50 W/m^2

6. Conclusions

A novel multirod solar-pumping approach with a Fresnel lens primary concentrator and Ce:Nd:YAG as gain media is proposed to increase the efficiency of solar-pumped lasers while making them more economically competitive. The solar laser head combines the light coupling capacity of the 3D-CPC with the ability of the conical cavity to confine the light through multiple reflections, ensuring efficient end-side pumping of the laser media. The proposed approach is designed and numerically analyzed through Zemax® 13 and LASCAD™ 3.3.5 tools, where different multirod configurations are optimized for the maximum extraction of solar laser power. The resultant thermal stress effects within the laser media are also investigated. The three-rod configuration enables the attainment of the highest total cw laser output power of 122.8 W, and, consequently, the highest solar-to-laser conversion efficiency of 7.31% and collection efficiency of 69.50 W/m^2, representing improvements of 1.88 times and 1.79 times, respectively, in relation to the records from the Ce:Nd:YAG/YAG single-rod solar laser with a Fresnel lens [25]. These results also contribute to enhancements of 1.58 times and 1.68 times over the solar-to-laser and collection efficiencies, respectively, of the highly efficient solar laser with three Ce:Nd:YAG rods [26]. Even so, the seven-rod configuration proves to be almost as efficient as the three-rod configuration, with the added advantage of being one of the configurations with the best thermal performance.

This work demonstrates that the combination of a Fresnel lens with an appropriate multirod pumping configuration using Ce:Nd:YAG laser media can be effective in developing cost-effective, solar-pumped lasers with a high efficiency and good thermal performance, creating more opportunities for their applications.

Author Contributions: Conceptualization, J.A., C.R.V. and D.L.; methodology, J.A., H.C. and D.L.; software, J.A, H.C., C.R.V. and D.L.; validation, J.A., H.C. and D.L.; formal analysis, J.A., H.C., C.R.V., B.D.T., A.M. and D.L.; investigation, J.A., H.C. and D.L.; resources, J.A., C.R.V. and D.L.;

data curation, J.A., H.C. and D.L.; writing—original draft preparation, J.A.; writing—review and editing, J.A., H.C., C.R.V., B.D.T., A.M. and D.L.; visualization, J.A.; supervision, D.L.; project administration, D.L.; funding acquisition, D.L. All authors have read and agreed to the published version of the manuscript.

References

1. Guan, Z.; Zhao, C.M.; Yang, S.H.; Wang, Y.; Ke, J.Y.; Zhang, H.Y. Demonstration of a free-space optical communication system using a solar-pumped laser as signal transmitter. *Laser Phys. Lett.* **2017**, *14*, 055804. [CrossRef]
2. DeYoung, R.J.; Walker, G.H.; Williams, M.D.; Schuster, G.L.; Conway, E.J. Preliminary design and cost of a 1-megawatt solar-pumped iodide laser space-to-space transmission station. *NASA Tech. Memo.* **1987**, *4002*, 27185. Available online: https://ntrs.nasa.gov/citations/19870017752 (accessed on 1 August 2023).
3. Abdel-Hadi, Y. Space-based solar laser system simulation to transfer power onto the earth. *NRIAG J. Astron. Geophys.* **2020**, *9*, 558–562. [CrossRef]
4. DeYoung, R.J.D.; Walberg, G.D.; Conway, E.J.; Jones, L.W. A NASA High-Power Space-Based Laser Research and Applications Program, IV. Ser. NASA SP-464. 1983. Available online: https://ntrs.nasa.gov/citations/19830018929 (accessed on 1 August 2023).
5. Vasile, M.; Maddock, C.A. Design of a Formation of Solar Pumped Lasers for Asteroid Deflection. *Adv. Space Res.* **2012**, *50*, 891–905. [CrossRef]
6. Johnson, C.S. Solar pumping converts broadband sunlight into efficient laser light. *Laser Focus World* **2022**, *58*, 10. Available online: https://www.laserfocusworld.com/lasers-sources/article/14283698/solar-pumping-converts-broadband-sunlight-into-efficient-laser-light (accessed on 1 August 2023).
7. Yabe, T.; Bagheri, B.; Ohkubo, T.; Uchida, S.; Yoshida, K.; Funatsu, T.; Oishi, T.; Daito, K.; Ishioka, M.; Yasunaga, N.; et al. 100 W-Class Solar Pumped Laser for Sustainable Magnesium-Hydrogen Energy Cycle. *J. Appl. Phys.* **2008**, *104*, 083104. [CrossRef]
8. Yan, B.; Li, Y.; Cao, W.; Zeng, Z.; Liu, P.; Ke, Z.; Yang, G. Efficient and Rapid Hydrogen Extraction from Ammonia–Water via Laser Under Ambient Conditions without Catalyst. *J. Am. Chem. Soc.* **2024**, *146*, 4864–4871. [CrossRef]
9. Motohiro, T.; Takeda, Y.; Ito, H.; Hasegawa, K.; Ikesue, A.; Ichikawa, T.; Higuchi, K.; Ichiki, A.; Mizuno, S.; Ito, T.; et al. Concept of the Solar-Pumped Laser-Photovoltaics Combined System and Its Application to Laser Beam Power Feeding to Electric Vehicles. *Jpn. J. Appl. Phys.* **2017**, *56*, 08MA07. [CrossRef]
10. Kiss, Z.J.; Lewis, H.R.; Duncan, R.C., Jr. Sun Pumped Continuous Optical Maser. *Appl. Phys. Lett.* **1963**, *2*, 93–94. [CrossRef]
11. Young, C.G. A Sun-Pumped cw One-Watt Laser. *Appl. Opt.* **1966**, *5*, 993–997. [CrossRef]
12. Arashi, H.; Oka, Y.; Sasahara, N.; Kaimai, A.; Ishigame, M. A Solar-Pumped cw 18 W Nd:YAG Laser. *Jpn. J. Appl. Phys.* **1984**, *23*, 1051–1053. [CrossRef]
13. Weksler, M.; Shwartz, J. Solar-pumped solid-state lasers. *IEEE J. Quantum Electron.* **1988**, *24*, 1222–1228. [CrossRef]
14. Lando, M.; Kagan, J.; Linyekin, B.; Dobrusin, V. A solar-pumped Nd:YAG laser in the high collection efficiency regime. *Opt. Commun.* **2003**, *222*, 371–381. [CrossRef]
15. Yabe, T.; Ohkubo, T.; Uchida, S.; Yoshida, K.; Nakatsuka, M.; Funatsu, T.; Mabuti, A.; Oyama, A.; Nakagawa, K.; Oishi, T.; et al. High-efficiency and economical solar-energy-pumped laser with Fresnel lens and chromium codoped laser medium. *Appl. Phys. Lett.* **2007**, *90*, 261120. [CrossRef]
16. Liang, D.; Almeida, J. Highly efficient solar-pumped Nd:YAG laser. *Opt. Express* **2011**, *19*, 26399–26405. [CrossRef] [PubMed]
17. Dinh, T.H.; Ohkubo, T.; Yabe, T.; Kuboyama, H. 120 watt continuous wave solar-pumped laser with a liquid light-guide lens and an Nd:YAG rod. *Opt. Lett.* **2012**, *37*, 2670–2672. [CrossRef]
18. Guan, Z.; Zhao, C.; Li, J.; He, D.; Zhang, H. 32.1 W/m^2 continuous wave solar-pumped laser with a bonding Nd:YAG/YAG rod and a Fresnel lens. *Opt. Laser Technol.* **2018**, *107*, 158–161. [CrossRef]
19. Mizuno, S.; Ito, H.; Hasegawa, K.; Suzuki, T.; Ohishi, Y. Laser emission from a solar-pumped fiber. *Opt. Express* **2012**, *20*, 5891–5895. [CrossRef]
20. Suzuki, Y.; Ito, H.; Kato, T.; Phuc, L.T.A.; Watanabe, K.; Terazawa, H.; Hasegawa, K.; Ichikawa, T.; Mizuno, S.; Ichiki, A.; et al. Continuous oscillation of a compact solar-pumped Cr, Nd-doped YAG ceramic rod laser for more than 6.5 h tracking the sun. *Sol. Energy* **2019**, *177*, 440–447. [CrossRef]
21. Masuda, T.; Iyoda, M.; Yasumatsu, Y.; Dottermusch, S.; Howard, I.A.; Richards, B.S.; Bisson, J.-F.; Endo, M. A Fully Planar Solar Pumped Laser Based on a Luminescent Solar Collector. *Commun. Phys.* **2020**, *3*, 60. [CrossRef]

22. Endo, M.; Yamamoto, K.; Dottermusch, S.; Howard, I.A.; Richards, B.S.; Tomizawa, R.; Masuda, T. Solar-pumped fiber laser using a solid-state luminescent solar collector. *Opt. Express* **2023**, *31*, 26040–26053. [CrossRef] [PubMed]

23. Vistas, C.R.; Liang, D.; Garcia, D.; Almeida, J.; Tibúrcio, B.D.; Guillot, E. Ce:Nd:YAG continuous-wave solar-pumped laser. *Optik* **2020**, *207*, 163795. [CrossRef]

24. Cai, Z.; Zhao, C.; Zhao, Z.; Zhang, J.; Zhang, Z.; Zhang, H. Efficient 38.8 W/m^2 Solar Pumped Laser with a Ce:Nd:YAG Crystal and a Fresnel Lens. *Opt. Express* **2023**, *31*, 1340–1353. [CrossRef] [PubMed]

25. Liang, D.; Almeida, J.; Catela, M.; Costa, H.; Garcia, D.; Tibúrcio, B.D.; Guillot, E.; Vistas, C.R. Lowest Threshold Solar-Pumped Ce:Nd:YAG Laser with 2.06% Solar-to-TEM$_{00}$ Mode Laser Conversion Efficiency. *Sol. Energy Mater. Sol. Cells* **2024**, *270*, 112817. [CrossRef]

26. Liang, D.; Vistas, C.R.; Garcia, D.; Tibúrcio, B.D.; Catela, M.; Costa, H.; Guillot, E.; Almeida, J. Most efficient simultaneous solar laser emissions from three Ce:Nd:YAG rods within a single pump cavity. *Sol. Energy Mater. Sol. Cells* **2022**, *246*, 111921. [CrossRef]

27. Almeida, J.; Liang, D.; Catela, M.; Costa, H.; Garcia, D.; Tibúrcio, B.D.; Guillot, E.; Vistas, C.R. Solar-Pumped Dual-Rod Ce:Nd:YAG Laser with 58 W Continuous-Wave Output Power and 5.1° Tracking Error Compensation Width. *Opt. Express* **2023**, *31*, 40041–40055. [CrossRef]

28. Sherniyozov, A.; Payziyev, S.; Begimqulov, S. Enhancing solar laser performance through multirod configurations. *J. Photon. Energy* **2024**, *14*, 024501. [CrossRef]

29. Liang, D.; Almeida, J.; Garcia, D.; Tibúrcio, B.D.; Guillot, E.; Vistas, C.R. Simultaneous Solar Laser Emissions from Three Nd:YAG Rods within a Single Pump Cavity. *Sol. Energy* **2020**, *199*, 192–197. [CrossRef]

30. Lupei, V.; Lupei, A.; Gheorghe, C.; Ikesue, A. Emission sensitization processes involving Nd^{3+} in YAG. *J. Lumin.* **2016**, *170*, 594–601. [CrossRef]

31. Wang, L.; Xia, C.; Xu, P.; Di, J.; Sai, Q.; Mou, F. Energy transfer in Ce, Nd, and Yb co-doped YAG phosphors. *Chin. Opt. Lett.* **2013**, *11*, 061604. [CrossRef]

32. Tai, Y.; Zheng, G.; Wang, H.; Bai, J. Near-infrared quantum cutting of Ce^{3+}–Nd^{3+} co-doped Y$_3$Al$_5$O$_{12}$ crystal for crystalline silicon solar cells. *J. Photochem. Photobiol. A* **2015**, *303–304*, 80–85. [CrossRef]

33. Payziyev, S.; Sherniyozov, A.; Bakhramov, S.; Zikrillayev, K.; Khalikov, G.; Makhmudov, K.; Ismailov, M.; Payziyeva, D. Luminescence sensitization properties of Ce:Nd:YAG materials for solar pumped lasers. *Opt. Commun.* **2021**, *499*, 127283. [CrossRef]

34. Garcia, D.; Liang, D.; Almeida, J.; Tiburcio, B.D.; Costa, H.; Catela, M.; Vistas, C.R. Elliptical-Shaped Fresnel Lens Design through Gaussian Source Distribution. *Energies* **2022**, *15*, 668. [CrossRef]

35. Xie, W.T.; Dai, Y.J.; Wang, R.Z.; Sumathy, K. Concentrated Solar Energy Applications Using Fresnel Lenses: A Review. *Renew. Sustain. Energy Rev.* **2011**, *15*, 2588–2606. [CrossRef]

36. Hornung, T.; Nitz, P. Optical loss due to diffraction by concentrator Fresnel lenses. *AIP Conf. Proc.* **2014**, *1616*, 63–66. [CrossRef]

37. Hornung, T.; Nitz, P. Light diffraction by concentrator Fresnel lenses. *Opt. Express* **2014**, *22*, A686–A704. [CrossRef]

38. Welford, W.T.; Winston, R. *High Collection Nonimaging Optics*, 1st ed.; Academic Press: New York, NY, USA, 1989. [CrossRef]

39. Heraeus Properties of Fused Silica. Heraeus Conamic | Heraeus Conamic-Properties. Available online: https://www.heraeus-conamic.com (accessed on 1 August 2023).

40. Liang, D.; Almeida, J.; Vistas, C.R.; Tibúrcio, B.D.; Garcia, D. Solar-Pumped Lasers. In *Green Energy and Technology*; Springer: Cham, Switzerland, 2023. [CrossRef]

41. *ASTM G173-03*; Standard Tables for Reference Solar Spectral Irradiances: Direct Normal and Hemispherical on 37° Tilted Surface. ASTM International: West Conshohocken, PA, USA, 2020. [CrossRef]

42. Payziyev, S.; Sherniyozov, A. Influence of thermal population of lower laser levels on the performance of end-side-pumped Ce:Nd:YAG solar laser. *J. Photon. Energy* **2022**, *12*, 044501. [CrossRef]

43. Payziyev, S.; Sherniyozov, A.; Bakhramov, S.; Parpiev, O.; Nurmatov, S.; Khalikov, G.; Payziyeva, D.; Begimkulov, S.A.; Kamoliddinov, F.M.; Aliboyev, A.; et al. Solar-pumped composite YAG/Ce:Nd:YAG/YAG laser with reduced thermal effects. *J. Photon. Energy* **2024**, *14*, 014501. [CrossRef]

44. Liang, D.; Almeida, J.; Tibúrcio, B.D.; Catela, M.; Garcia, D.; Costa, H.; Vistas, C.R. Seven-Rod Pumping Approach for the Most Efficient Production of TEM$_{00}$ Mode Solar Laser Power by a Fresnel Lens. ASME. *J. Sol. Energy Eng.* **2021**, *143*, 061004. [CrossRef]

45. Vistas, C.R.; Liang, D.; Catela, M.; Costa, H.; Garcia, D.; Tibúrcio, B.D.; Almeida, J. Fresnel Lens Solar Pumping for Uniform and Stable Emission of Six Sustainable Laser Beams under Non-Continuous Solar Tracking. *Sustainability* **2023**, *15*, 8218. [CrossRef]

46. Tibúrcio, B.D.; Liang, D.; Almeida, J.; Garcia, D.; Catela, M.; Costa, H.; Vistas, C.R. Fresnel Lens Solar-Pumped Laser with Four Rods and Beam Merging Technique for Uniform and Stable Emission under Tracking Error Influence. *Energies* **2023**, *16*, 4815. [CrossRef]

47. Costa, H.; Liang, D.; Matos, A.; Almeida, J. Multi-Fresnel-Lens Pumping Approach for Simultaneous Emission of Seven TEM$_{00}$-Mode Beams with 3.73% Conversion Efficiency. *Photonics* **2024**, *11*, 889. [CrossRef]